CLIMATE FORCING

No consistent ENSO response to volcanic forcing over the last millennium

Sylvia G. Dee[1]*, Kim M. Cobb[2], Julien Emile-Geay[3], Toby R. Ault[4], R. Lawrence Edwards[5], Hai Cheng[6,5], Christopher D. Charles[7]

The El Niño–Southern Oscillation (ENSO) shapes global climate patterns yet its sensitivity to external climate forcing remains uncertain. Modeling studies suggest that ENSO is sensitive to sulfate aerosol forcing associated with explosive volcanism but observational support for this effect remains ambiguous. Here, we used absolutely dated fossil corals from the central tropical Pacific to gauge ENSO's response to large volcanic eruptions of the last millennium. Superposed epoch analysis reveals a weak tendency for an El Niño–like response in the year after an eruption, but this response is not statistically significant, nor does it appear after the outsized 1257 Samalas eruption. Our results suggest that those models showing a strong ENSO response to volcanic forcing may overestimate the size of the forced response relative to natural ENSO variability.

Detecting forced changes in El Niño–Southern Oscillation (ENSO) variability is a formidable challenge, requiring centuries of data beyond the range of the instrumental record (*1*, *2*). Indeed, tropical Pacific variability documented by instrumental and satellite observations spans only a century and a half at the very most, but it can be extended using paleoclimate archives from the relatively data-rich last millennium (hereafter LM). Recent work using both paleoclimate data and climate models has searched for forced changes to ENSO over the LM, evaluating the response of the tropical Pacific to external forcing over longer time scales. In particular, a large body of recent modeling studies suggest that global cooling associated with explosive volcanism can initiate an El Niño–like response in the tropical Pacific up to 2 years after the eruption. In models, this response is linked to basin-scale cooling patterns that drive an equatorward shift of the Intertropical Convergence Zone, which favors weaker trade winds in the western and central tropical Pacific (*2*–*4*), changes in the zonal sea surface temperature (SST) gradients with cooling in the west and a reduction in mean upwelling typically associated with an El Niño event [consistent with a dynamical thermostat mechanism (*5*–*7*)]. Still other studies invoke substantial cooling over tropical Africa (*8*) as a means for initiating a tropical warming response through perturbations to the Walker circulation. In all cases, the modeled response additionally depends on the background ENSO state during the time of the eruption and the eruption size (*6*, *9*), with a potential influence from the season in which the eruption occurs (*10*). In general, these massive volcanic eruptions provide an opportunity to test climate system and model sensitivity to sulfate aerosol forcing, offered as a possible geoengineering strategy for offsetting greenhouse warming (*11*).

The response to LM external forcing as recorded by paleoclimate data is documented in previous work (*2*, *12*–*16*), but most such studies rely on teleconnected responses outside the core ENSO region. Coral oxygen isotopic records from the northern Line Islands have yielded monthly resolved, high-fidelity records of past ENSO variability (*17*–*20*), recording SST variability in the heart of the central tropical Pacific. Correlation coefficients for Christmas, Fanning, and Palmyra island coral records and the NINO3.4 SST index are –0.92, –0.85, and –0.82, respectively, on interannual time scales (*19*), demonstrating high sensitivity to ENSO (*17*, *18*).

Here, we present measurements of oxygen isotopes in two fossil coral segments that bridge previously published Palmyra coral reconstructions (*18*) to constitute 319 years of absolutely dated, continuous, submonthly resolved coral $\delta^{18}O$ data extending from 1146 to 1465 CE (Fig. 1). The full record is composed of eight overlapping corals, with 75% of the time series generated from measurements of more than

[1]Rice University, Department of Earth, Environmental, and Planetary Sciences, Houston, TX 77005, USA. [2]School of Earth and Atmospheric Sciences, Georgia Institute of Technology, Atlanta, GA 30332, USA. [3]Department of Earth Sciences, University of Southern California, Los Angeles, CA 90089, USA. [4]Department of Earth and Atmospheric Sciences, Cornell University, Ithaca, NY 14853, USA. [5]Department of Earth Sciences, University of Minnesota, Minneapolis, MN 55455, USA. [6]Institute of Global Environmental Change, Xi'an Jiaotong University, Xi'an 710054, China. [7]Scripps Institution of Oceanography, San Diego, CA 92037, USA.
*Corresponding author. Email: sylvia.dee@rice.edu

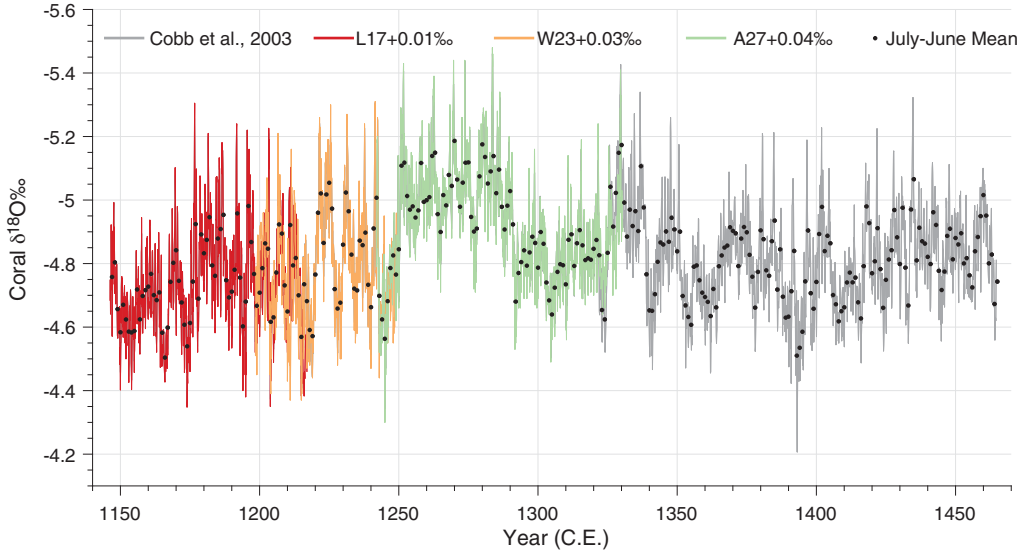

Fig. 1. Coral oxygen isotopes from Palmyra island. Shown are monthly resolved fossil coral oxygen isotopes measured in the multisegment Palmyra corals spanning the LM. This work highlights three new segments added to a monthly resolved, continuous eight-coral splice spanning three centuries of tropical Pacific oxygen isotope variability. The *y*-axis is inverted given that El Niño events drive negative $\delta^{18}O$ excursions in the coral data. U-Th dating places a bottom date in the coral segment of 1147 CE, and residual errors compound exponentially before and after this date horizon (see materials and methods section S1 and fig. S1). Annual means (black) are calculated as 1 July to 30 June averages to center coral annual averages on peak ENSO extremes that occur in December–January–February. Adjustments in mean offsets between segments are detailed in table S3.

one coral segment. The high reproducibility of overlapping segments bolsters our confidence in both the fidelity of the climate signal embedded in these records, as well as the accuracy of the individual coral uranium-thorium (U-Th) age models (see materials and methods sections S1.1 and S1.2). Eleven new high-precision U-Th dates yield age control for the bridging segments such that, in combination with the previously published dates (*18*), chronological errors are reduced to σ = ±1 year, rivaling the precision of the most well-replicated ice-core and tree-ring chronologies (*21*) (see materials and methods sections S1.1 and S1.2, tables S1 and S2, and figs. S1 and S2). Note that offsets in the mean values of coral $\delta^{18}O$ are reported in both Fig. 1 and section S1.2, but are not relevant to the analyses presented herein, which rely on interannual changes in coral $\delta^{18}O$, not the absolute value of a given sequence. The new composite coral $\delta^{18}O$ record represents the longest, best replicated, highest-resolution, and most proximal record to the center of ENSO variability currently available and presents a window into the effects of large volcanic eruptions on tropical Pacific climate.

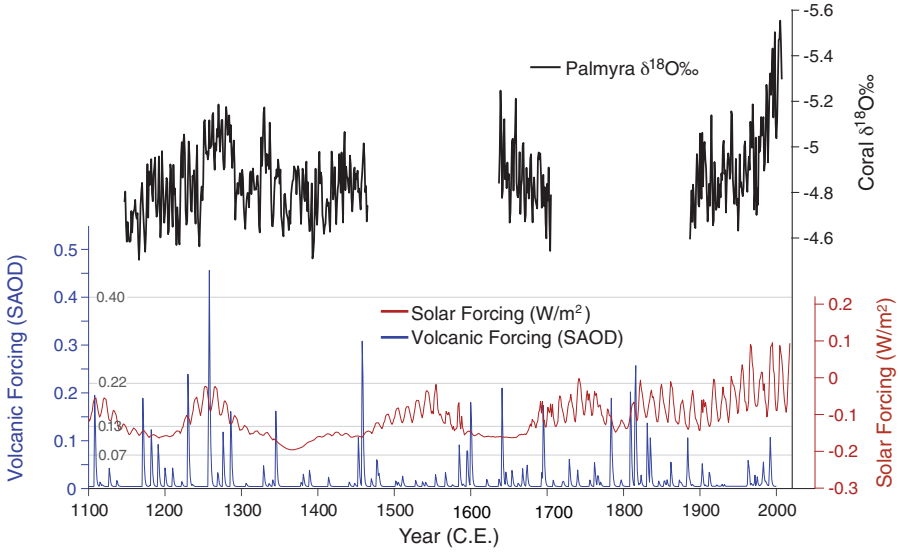

Fig. 2. External forcing and the Palmyra coral record over the LM. Reconstructed volcanic eruption dates reconstructed through SAOD (unitless) from (*22*) (blue), as well as the average LM solar-forcing reconstruction (red) (*36*) plotted with the full Palmyra $\delta^{18}O$ record (black), with individual segments spanning 1147 to 1998 CE. The modern coral piece spans 1887 to 1998 CE; earlier segments are measurements from fossil corals. The *y*-axis is inverted given that El Niño events drive negative $\delta^{18}O$ excursions in the coral data. Coral annual means (black) are calculated as 1 July to 30 June averages to center data across the largest ENSO anomalies. Volcanic-forcing thresholds are marked corresponding to SAOD exceeding 0.07, 0.13, 0.22, and 0.43 (gray lines).

Table 1. Ten largest volcanic eruptions intersecting coral data. Scaling from SAOD to radiative forcing (RF, in W/m^2) differs between reconstructions (*21*, *22*). Both are scaled as a function of sulfate measurements from ice cores. Shown are eruptions that occur in the tropics (latitude within [20°S;20°N], if known) and that intersect coral data over the LM. The top six largest eruption years intersecting the coral data are shown in Fig. 3. For reference, an AOD of 0.01 represents a clear atmosphere and 0.4 is extremely hazy.

Year (CE)	eVolv2k		Sigl *et al.* (2015)
	SAOD	RF (W/m^2)	RF (W/m^2)
1258	0.46	−11.39	−32.8
1458	0.31	−7.7	−20.6
1230	0.24	−5.97	−15.9
1641	0.21	−5.24	−11.8
1171	0.19	−4.73	−11.3
1695	0.17	−4.35	−10.2
1345	0.16	−4.05	−9.4
1286	0.16	−4.03	−9.7
1182	0.12	−3.09	−5.6
1276	0.12	−2.94	−7.7

This work tests the hypothesis that volcanic-induced cooling may initiate a dynamical response leading to an "El Niño–like" tropical Pacific anomaly (*2*–*4*, *6*–*8*). The newly generated multicentury coral splice spanning the 12th to the 15th century improves our ability to diagnose the role of volcanic activity in shaping tropical Pacific climate during the LM and allows us to reevaluate the response of the tropical Pacific to external forcing using the latest reconstructions of volcanic forcing (*21*, *22*) (Fig. 2 and fig. S7). In particular, the corals span several of the largest tropical eruptions of the LM (Table 1), including the 1257 CE Samalas eruption (*23*). Samalas was the largest and most sulfurous eruption of the LM, with about twice the sulfate aerosol emissions as the 1815 CE eruption of Mt. Tambora (*16*). The full record, composited from multiple cores, covers 564 years of the period 1150 to 1998 CE (Figs. 1 and 2) and samples 26 tropical volcanic eruptions. ENSO variability at Palmyra is captured as low-$\delta^{18}O$ anomalies corresponding to warm, wet, El Niño–like conditions and high-$\delta^{18}O$ anomalies corresponding to cool, dry, La Niña–like conditions; thus, the hypothesis as posed tests for lower $\delta^{18}O$ in the 1- to 3-year period after tropical volcanic eruptions. In combination with the longevity and central Pacific location of the Palmyra Island corals, the data offer a good opportunity for independent analysis of the model results.

Coral sensitivity to tropical volcanic forcing over the past ~900 years is examined using the evolv2k volcanic aerosol reconstruction (Fig. 2) (*21*, *22*). Using sulfate aerosols in laminated ice cores, the reconstruction yields improved estimates of eruption date and forcing magnitude using multiparameter measurements (*21*). These enable reconstructions of stratospheric aerosol optical depth (SAOD), a dimensionless measure of the extinction of downwelling sunlight by aerosol particles in a given vertical column of the atmosphere. Volcanic reconstructions differ in their scaling parameterization of SAOD to estimate radiative forcing (see materials and methods section S1.5 and fig. S6). Furthermore, uncertainties remain as to the amount of sulfate aerosols present in ice cores that actually penetrates the stratosphere (*24*). Thus,

we circumvent these uncertainties by focusing solely on eruption timing as derived from ice-core chemistry. Volcanic eruptions are defined as local maxima across SAOD values reported in the ice-core reconstructions. The top 10 eruptions of the LM in terms of SAOD and estimated radiative forcing are given in Table 1.

Of the six largest eruptions of the LM intersecting the coral data (Fig. 3), four show a shift toward more negative (thus, El Niño–like) anomalies in the year after the eruption. To isolate the coral response to all tropical eruptions, we used superposed epoch analysis (SEA) (see materials and methods section S1.4). Previous work using intermediate complexity models of ENSO indicate that only large eruptions with forcing less than –3.7 W/m^2 increase the likelihood of initiating an El Niño response (*6*). To assess the sensitivity of our findings to the eruption magnitude and reconstruction uncertainties, the volcanic radiative–forcing threshold was systematically varied (SAOD > 0.07, 0.13, 0.22, and 0.43), testing the assumption that eruption size affects the detection of a significant response in the corals (see materials and methods section S1.4 and Fig. 4). For reference, the 1991 eruption of Mt. Pinatubo resulted in an estimated SAOD of 0.11. These thresholds scale to a radiative forcing of approximately –1.5, –3, –5, and –10 W/m^2, respectively, using the SAOD conversion reported in (*22*). As forcing threshold increases, the number of eruptions of sufficient magnitude intersecting the coral data sharply decreases from 26 to 1 (the 1257 CE eruption only) (Fig. 4), which complicates evaluation of statistical significance. In particular, the small sample size affects the probability of incorrect retention of the null hypothesis, a "type II error." This issue was circumvented by applying a block bootstrap resampling of the coral data in the SEA composite matrix, drawing only from no-eruption years (see materials and methods sections S1.3 and S1.4). This assesses volcanic responses against the null hypothesis of a stationary stochastic process in which no eruption occurs.

For the SEA composite across eruptions exceeding an AOD of 0.13 (1230, 1257, 1458, and 1641 CE), we observe El Niño–like anomalies in the year after the eruption, close to, but under, the 95% confidence level (Fig. 4C). As a result, we cannot confirm or deny the presence of a post-eruption warming at this level; there may be a response for sufficiently large eruptions but large internal variability obscures detection of a significant signal. Although a single composite response (Fig. 4C) grazes the uncertainty bounds, across all eruption thresholds, none of the coral responses was significant at the 95% confidence level. Thus, whereas SEA composite means of the post-eruption δ^{18}O anomalies (Fig. 4, C and D) do show an El Niño–like shift in coral δ^{18}O values after large volcanic eruptions, the response is indistinguishable from unforced (endogenous) variability. The coral data neither confirm nor refute a shift in the occurrence of ENSO anomalies after volcanic eruptions, even for the largest events. This result was replicated and confirmed using three additional volcanic reconstructions (*21*, *25*, *26*) (see materials and methods section S1.5 and fig. S7).

This analysis suggests that the influence of external forcing on ENSO is either absent or difficult to detect over the past millennium. The impacts of external forcing (and the reconstructions of these forcings) on ENSO in climate models are still uncertain, but paleoclimate archives from Palmyra island provide independent validation for model simulations. Despite the fossil corals' demonstrated high sensitivity to ENSO variability and mean state (*15*, *18*), the record shows no significant sensitivity to volcanic forcing on interannual to decadal time scales. Our result holds for the largest known volcanic events of the LM, including those in 1230, 1257, 1458, and 1641 CE; all of these eruptions have an SAOD >0.22, twice as large as the 1991 Pinatubo eruption. The Palmyra data do shift toward warmer temperatures in the eruption year and the following 2 years, with coral δ^{18}O anomalies consistent with an El Niño–like response to sufficiently explosive volcanism. However, uncertainty quantification suggests that the data do not support the hypothesis that large volcanic events trigger a detectable response in central Pacific climate.

To directly compare available model simulations of ENSO's response to volcanic forcing to the fossil corals, Fig. 4 shows the same analysis for the Paleoclimate Modeling Intercomparison Project (PMIP3) and Community Earth

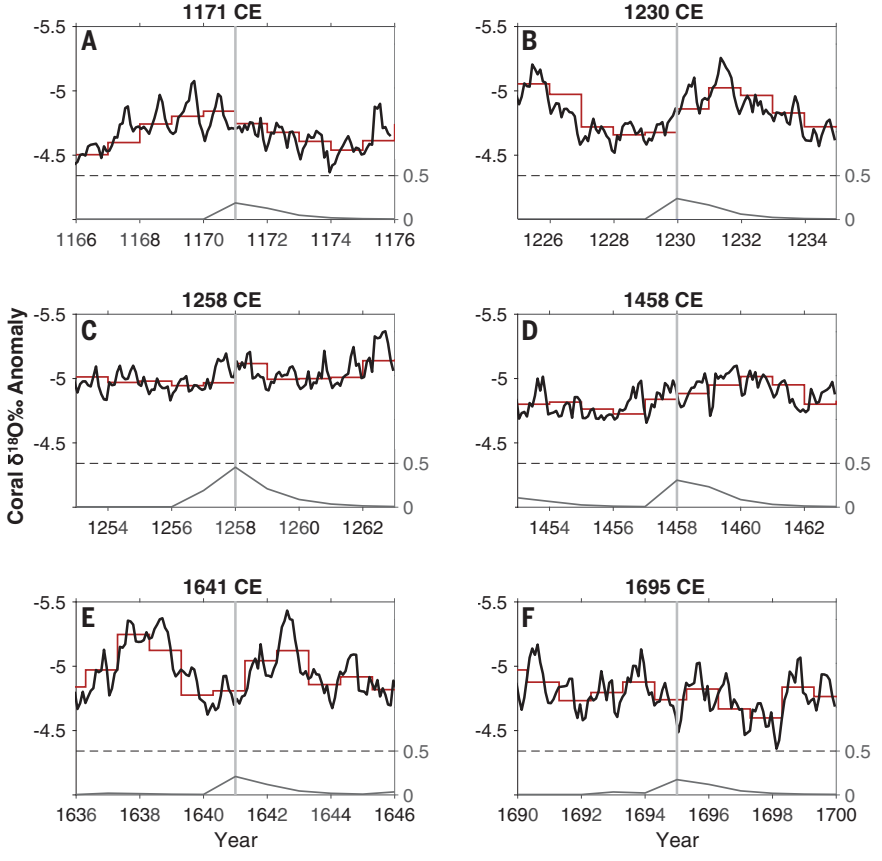

Fig. 3. Coral δ^{18}O monthly measured values across the largest eruptions of the LM (forcing < –10 W/m^2: 1171, 1230, 1258, 1458, 1641, and 1695). (**A**) to (**F**) show the Palmyra record coral annual average (dark red) and monthly values (black) plotted across each eruption. The *y*-axis is inverted such that warm events (which drive negative δ^{18}O) are above zero in the figure. Annual means (dark red) are calculated as 1 July to 30 June averages to center coral annual averages on peak ENSO extremes that occur in December–January–February. Gray lines show the respective SAOD forcing for each eruption, as well as the timing of the SAOD maxima (vertical gray lines intersecting coral time series).

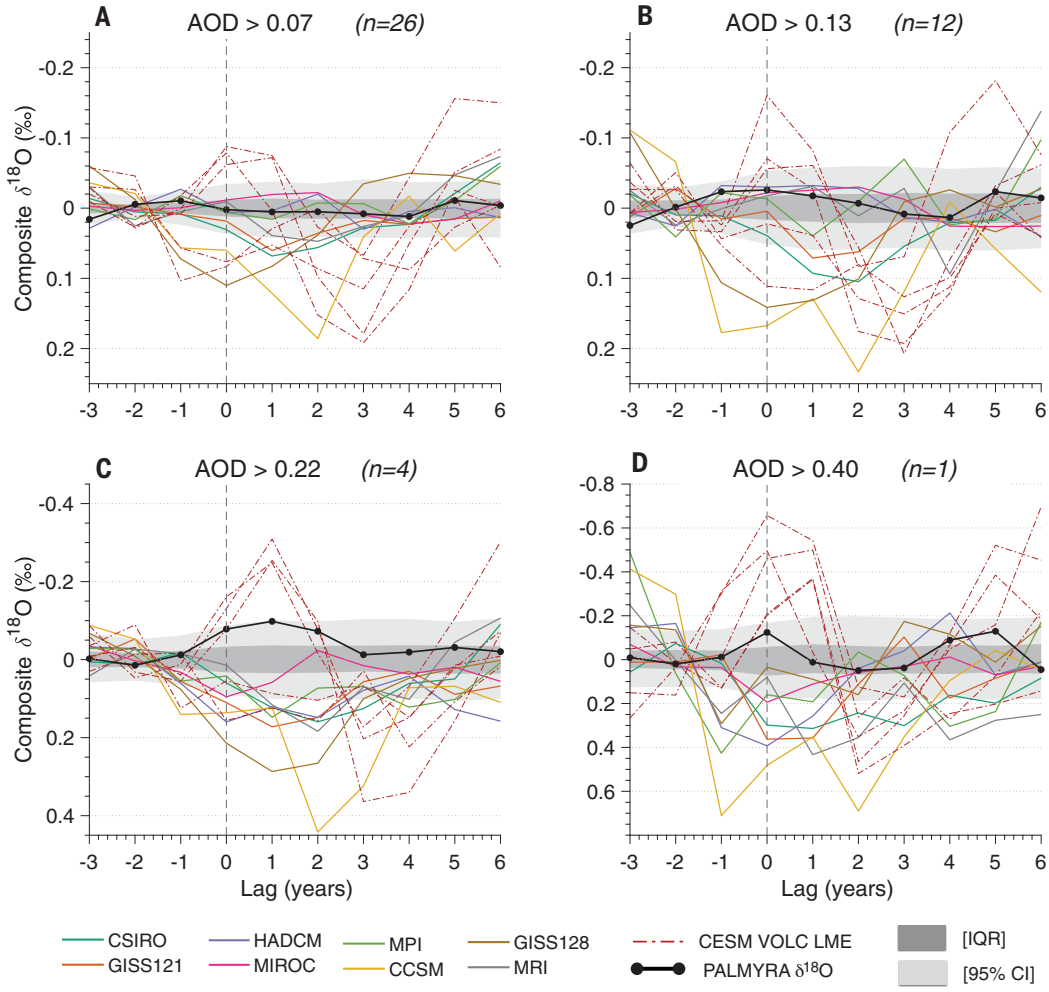

Fig. 4. Superposed epoch analysis for coral data intersecting with eruptions as defined in the Toohey *et al.* (2017) volcanic-forcing reconstruction. Composite $\delta^{18}O$ response for the 3 years before and 6 years after all eruptions exceeding a given forcing threshold (see materials and methods). The *y*-axis is inverted such that El Niño events (which drive negative $\delta^{18}O$ at Palmyra) correspond to upward excursions. (**A**) AOD > 0.07 (26 eruptions), (**B**) AOD > 0.12 (12 eruptions), (**C**) AOD > 0.22 (1230, 1257, 1458, and 1641 CE), (**D**) AOD > 0.43 (1257 CE; Samalas only); note the different *y*-axis for (C) and (D) because of the large model response curve. SEA averages over the *n* events that exceed the specified AOD threshold for each case [(D); AOD > 0.40] includes only the 1257 CE Samalas eruption. Light gray–shaded areas show the 50% and 95% highest-density regions from block bootstrap resampling of noneruption years (for comparison). Only excursions falling outside these intervals may be deemed significant at the 95% confidence level. Dark gray shading indicates middle 50% [0.25–0.75] interquartile range of the block bootstrap ensemble (IQR). Before evaluating the coral response to volcanic events, a 2- to 7-year bandpass filter was applied to emphasize canonical ENSO variability. Also plotted are the PMIP3 (solid colors) and CESM-LME volcanic forcing (dashed red lines) simulations for the same eruption thresholds, mapped to $\delta^{18}O$ space through the forward model of (*28*, *37*) (see materials and methods). Note that various simulations used different volcanic-forcing reconstructions (*25*, *26*) (see table S5), contributing to differences in their composite response.

System Model Last Millennium Ensemble [CESM-LME (*27*)] volcanic-forcing ensemble members. (For clarity, we note that this analysis is specific to this study and is independent of literature cited in this work evaluating model responses to volcanism.) The climate model simulations were processed identically to the coral data by extracting monthly Niño 3.4 region SST anomalies, computing anomalies relative to the monthly mean seasonal cycle, and applying the SST-scaling conversion for Porites corals (Fig. 4 caption, materials and methods section S1.6, and fig. S8). For completeness, the model conversion was repeated using a full proxy system model for coral $\delta^{18}O$, which considers the joint impacts of temperature and hydroclimate (*28*) (see materials and methods section S1.6 and fig S9). The model simulations generally exhibit a stronger, though highly variable, response to volcanism. The PMIP3 ensemble responses are inconsistent in that many models exhibit a muted response to volcanism, whereas others exhibit large post-eruption cooling in years 2 to 3 (*7*). By contrast, the mean of the CESM-LME ensemble members indicates substantial warming in years 0 to 1, as described in (*2*). For AOD thresholds >0.13 (corresponding to forcing ≤−3: −5 W/m^2), most models' temperature response to volcanic eruptions is characterized by a larger post-eruption variability than that of the corals. For CESM, the warming response is larger than the coral response for all eruption magnitude thresholds (Fig. 4). This result is robust to multiple SST-coral conversions (see materials and methods section S1.6 and figs. S8 and S9) (*29*).

Taken together, our results show that tropical Pacific SSTs as recorded by $\delta^{18}O$ of Palmyra corals are broadly insensitive to changes in radiative forcing given SEA across several AOD thresholds. There is a coral $\delta^{18}O$ response consistent with El Niño–like conditions detected below the 95% confidence level for large eruptions, but it is absent for the 1257 CE eruption of Samalas, the largest of the LM. These results imply that if the dynamical links between LM volcanism and tropical Pacific state suggested by climate models (*2*–*4*, *7*) do exist in the real world, their impact is small relative to natural variability, and potentially overestimated in some models. This is consistent with the claim that most, if not all, of the variability exhibited by ENSO over the preindustrial portion of the LM is linked to endogenous climate variability.

Volcanism's impact in the tropical Pacific in climate models is characterized by a high variance response and, in some cases, a strong warming or cooling in the central tropical

Pacific (Fig. 4). The Palmyra data, which show no significant change in the frequency, occurrence, or magnitude of El Niño events nor a significant change in central tropical Pacific $\delta^{18}O$, thus highlight an important data-model discrepancy surrounding the sensitivity of the tropical Pacific to external forcing. The broad range of model responses shown in Fig. 4 underscores structural uncertainties in model forcing and/or physics. Directly addressing uncertainties surrounding the size and partitioning between tropospheric and stratospheric aerosols during volcanic events, new high-resolution sulfur isotope measurements that differentiate between sulfate aerosols derived from stratospheric intrusions are poised to refine forcing estimates from ice cores spanning the LM (*24*). Additionally, mounting evidence suggests that volcanic forcing used to drive current-generation climate models is up to 67% too large because of structural uncertainties in stratospheric aerosol physics (*30*). This results in overestimated responses to volcanism in terms of intensity and longevity (*31*). Forthcoming improvements to the volcanic forcing applied in models may result in a weaker climatic response to a given aerosol loading (*30*).

Furthermore, recent work has shown that eruption season may prove as important as eruption magnitude in shaping the response of tropical Pacific climate to volcanic forcing (*10*), complicating data-model comparison. Many model simulations assume that all eruptions occur in a single month [e.g., January (*21*, *22*) or April (*25*)], which introduces uncertainties in the response with respect to proxy signatures of real-world eruptions. As highlighted in (*10*), multiproxy tropical temperature reconstructions lend some support for a warming response in the year after a tropical eruption, but data from moisture-sensitive trees in ENSO-teleconnected regions yield evidence of tropical Pacific cooling. In assessing these lines of evidence, we note that the volcanic response of extratropical tree ring width reflects two or more confounding sources: (i) local changes in precipitation caused by the direct radiative cooling from volcanic events (*32*) and (ii) changes in ENSO state, whether they be endogenous to the tropical Pacific or induced by volcanism. Moreover, a modeling study suggests that these two responses bear a close resemblance to each other (*2*). Such studies highlight the importance of using proximal records of tropical Pacific state, such as that presented in this work, to assess the relationship between volcanism and ENSO.

Climate model predictions of the climate system's response to continued greenhouse emissions depend crucially on accurate simulation of ENSO's response to external forcing. Recent work suggests that recent ENSO properties reflect a sensitivity to anthropogenic forcing (*19*, *20*, *33*), a finding supported by select climate models simulations of future climate change (*34*, *35*). Both modeling and data-based assessments of climate change impacts on ENSO must overcome the high degree of intrinsic variability, a detection threshold that is not met in the present study with respect to volcanic forcing. Whereas models can rely on ensembles to elevate signal-to-noise ratios, in the paleoclimate record, as in reality, we are limited to one realization. This ultimately limits our ability to detect changes in ENSO derived from model-based targets. However, the sign, structure, and magnitude differ between volcanic versus greenhouse forcing, ultimately limiting the relevance of the volcanic-forcing response of ENSO to potential responses of ENSO to greenhouse gas forcing.

Finally, this work highlights a role for high-resolution paleoclimate reconstructions and model simulations of LM volcanism in the assessment of potential geoengineering schemes designed to offset greenhouse warming in coming decades. There are few results from natural experiments available that facilitate investigations of the climate system response to sulfate aerosol loading. The volcanic response of major climate modes such as ENSO is key to assessing regional climate impacts under solar radiation management scenarios. As such, our work suggests that continued efforts toward data-model comparisons of the effects of volcanic eruptions on regional climate over the LM are critical to a robust assessment of the climatic effects of sulfate aerosol–induced geoengineering scenarios.

REFERENCES AND NOTES

1. A. T. Wittenberg, *Geophys. Res. Lett.* **36**, L12702 (2009).
2. S. Stevenson, B. Otto-Bliesner, J. Fasullo, E. Brady, *J. Clim.* **29**, 2907–2921 (2016).
3. F. S. R. Pausata, L. Chafik, R. Caballero, D. S. Battisti, *Proc. Natl. Acad. U S A* **112**, 13784–13788 (2015).
4. F. S. R. Pausata, C. Karamperidou, R. Caballero, D. S. Battisti, *Geophys. Res. Lett.* **43**, 8694–8702 (2016).
5. M. E. Mann, M. A. Cane, S. E. Zebiak, A. Clement, *J. Clim.* **18**, 447–456 (2005).
6. J. Emile-Geay, R. Seager, M. Cane, E. Cook, G. H. Haug, *J. Clim.* **21**, 3134–3148 (2008).
7. N. Maher, S. McGregor, M. H. England, A. S. Gupta, *Geophys. Res. Lett.* **42**, 6024–6033 (2015).
8. M. Khodri *et al.*, *Nat. Commun.* **8**, 778 (2017).
9. F. Lehner, A. P. Schurer, G. C. Hegerl, C. Deser, T. L. Frölicher, *Geophys. Res. Lett.* **43**, 2851–2858 (2016).
10. S. Stevenson, J. T. Fasullo, B. L. Otto-Bliesner, R. A. Tomas, C. Gao, *Proc. Natl. Acad. Sci. U.S.A.* **114**, 1822–1826 (2017).
11. M. Plazzotta, R. Séférian, H. Douville, B. Kravitz, J. Tjiputra, *Geophys. Res. Lett.* **45**, 5663–5671 (2018).
12. J. Brad Adams, M. E. Mann, C. M. Ammann, *Nature* **426**, 274 (2003).
13. K. Anchukaitis *et al.*, *Geophys. Res. Lett.* **37**, n/a (2010).
14. J. Li *et al.*, *Nat. Clim. Chang.* **3**, 822–826 (2013).
15. J. Emile-Geay, K. M. Cobb, M. E. Mann, A. T. Wittenberg, *J. Clim.* **26**, 2302–2328 (2013).
16. S. Guillet *et al.*, *Nat. Geosci.* **10**, 123–128 (2017).
17. K. M. Cobb, C. D. Charles, D. E. Hunter, *Geophys. Res. Lett.* **28**, 2209–2212 (2001).
18. K. M. Cobb, C. D. Charles, H. Cheng, R. L. Edwards, *Nature* **424**, 271–276 (2003).
19. K. M. Cobb *et al.*, *Science* **339**, 67–70 (2013).
20. P. R. Grothe *et al.*, *Geophys. Res. Lett.* (2019); https://doi.org/10.1029/2019GL083906.
21. M. Sigl *et al.*, *Nature* **523**, 543–549 (2015).
22. M. Toohey, M. Sigl, *Earth Syst. Sci. Data* **9**, 809–831 (2017).
23. F. Lavigne *et al.*, *Proc. Natl. Acad. Sci. U.S.A.* **110**, 16742–16747 (2013).
24. A. Burke *et al.*, *Earth Planet. Sci. Lett.* **521**, 113–119 (2019).
25. C. Gao *et al.*, *J. Geophys. Res. Atmos.* **111** (D12), D12107 (2006).
26. T. J. Crowley *et al.*, *PAGES News* **16**, 22–23 (2008).
27. B. L. Otto-Bliesner *et al.*, *Bull. Am. Meteorol. Soc.* **97**, 735–754 (2016).
28. S. Dee *et al.*, *J. Adv. Model. Earth Syst.* **7**, 1220–1247 (2015).
29. In the case of the Samalas eruption (Fig. 4D), models show a warming in the eruption year; note that simulated NINO34 indices were annually averaged from July 1 to June 30 to center the winter El Niño response (as in the coral data). CESM applies volcanic forcing in April of each calendar year (*2*, *25*), and thus the 'year 0' response is a by-product of the time-averaging method.
30. A. N. LeGrande, K. Tsigaridis, S. E. Bauer, *Nat. Geosci.* **9**, 652–655 (2016).
31. M. Stoffel *et al.*, *Nat. Geosci.* **8**, 784–788 (2015).
32. A. Meyer, D. Folini, U. Lohmann, T. Peter, *J. Clim.* **29**, 1325–1338 (2016).
33. Y. Liu *et al.*, *Nat. Commun.* **8**, 15386 (2017).
34. W. Cai *et al.*, *Nat. Clim. Chang.* **5**, 849–859 (2015).
35. W. Cai *et al.*, *Nature* **564**, 201–206 (2018).
36. G. A. Schmidt *et al.*, *Geosci. Model Dev.* **4**, 33–45 (2011).
37. D. M. Thompson, T. R. Ault, M. N. Evans, J. E. Cole, J. Emile-Geay, *Geophys. Res. Lett.* **38**, L14706 (2011).

ACKNOWLEDGMENTS

We thank M. Toohey for assistance with the evolv2k dataset, A. LeGrande and J. Russell for valuable insights on this work, and P. Grothe for assistance with coral chronological assignments. **Funding:** This research was supported by the Peter Voss Postdoctoral Fellowship in the Institute at Brown for Environment and Society, Brown University, as well as the University of Texas at Austin, Institute for Geophysics Postdoctoral Fellowship, both awarded to S.D.; by NSF Marine Geology and Geophysics awards 0752091, 1502832, and 1836645 to K.C.; NSF OCE award 0752585 to C.D.C. and K.C.; and NOAA grant NA18OAR4310426 to J.E.G. **Author contributions:** S.D., K.C., J.E.G., and T.A. formulated research questions. K.C. and C.D.C. collected, sampled, and analyzed oxygen isotopes in the coral data with assistance from L.E. and H.C. S.D. performed analysis on coral data, generated figures, and extracted model output with guidance from K.C., J.E.G., and T.A. All authors contributed to the writing of the manuscript. **Competing interests:** The authors declare no competing interests. **Data and materials availability:** All data and code are available in the supplementary materials and are publicly available on the National Climatic Data Centers website at https://www.ncdc.noaa.gov/paleo/study/27490.

SUPPLEMENTARY MATERIALS

science.sciencemag.org/content/367/6485/1477/suppl/DC1
Section S1: Materials and Methods
Section S2: Data and Matlab Code
Tables S1 to S5
Figs. S1 to S9
References (*38*–*48*)

1 March 2019; accepted 2 March 2020
10.1126/science.aax2000